ChemPhysChem
Research Article
doi.org/10.1002/cphc.202400950
Chemistry Europe
European Chemical Societies Publishing
www.chemphyschem.org

# Structural Investigation and Enriched Catalysis of Cu-Complex-Encapsulated Microporous Catalyst with Pragmatic Modeling for Prediction of Activity by Using Machine Learning

Rohit Prajapati, Jetal Chaudhari, Parikshit Paredi, Daksh Vyawhare, Nao Tsunoji, Rayan Bandyopadhyay, Krupa Shah,* Rajib Bandyopadhyay,* and Mahuya Bandyopadhyay*

Silicoaluminophosphates (SAPOs) are structurally diverse materials widely used in separation, catalysis, and environmental applications. In this study, a simple post-synthetic method is used to create a hybrid porous material by immobilizing a copper(II) complex onto base-functionalized SAPO molecular sieves. The copper complex, synthesized using 2,9-dimethyl-1,10-phenanthroline and copper nitrate, is structurally confirmed through single-crystal X-ray diffraction. The effective activity in ring-opening reaction of epoxide is achieved when this complex is anchored on amine-functionalized SAPO materials. Characterization techniques such as powder X-ray diffraction, $N_2$ adsorption-desorption, Fourier transform infrared spectroscopy, nuclear magnetic resonance, scanning electron microscope, and thermogravimetric analysis confirm the structural integrity, surface properties, and thermal stability of the materials. High conversion efficiencies of 90% and 88% are achieved using copper-complex-immobilized SAPO-34 and SAPO-5, respectively. To enhance industrial applicability, machine learning techniques are applied to predict product conversion and selectivity. Methods such as linear regression, support vector machine (SVM), and k-nearest neighbors (kNN) are evaluated, with SVM and kNN showing strong predictive performance. Error metrics like mean-squared error, mean absolute percentage error, and R score validate the model accuracy. This work highlights the effective integration of functionalized SAPOs with ML tools for catalytic optimization and industrial-scale applications.

## 1. Introduction

The research field of heterogeneous catalysis has a long history, attracting interest due to the abundance of catalysts and being one of the most significant industrial processes in chemical manufacturing.[1–3] The relevance of porous materials in newly developed energy storage and conversion devices has been recognized.[4] Most studies have concentrated on pore-structure tailoring by optimizing preparation processes, which possess a broad array of applications including catalysis, separation, insulation, sensors, chromatography, etc.[5,6] A particular kind of molecular sieve or zeolite called silicoaluminophosphate (SAPO) has been the subject of much study and development because of its special qualities and uses in the petrochemical and refining industries.[7–9] The functionality of microporous materials is diverse and extends across multiple disciplines, making them essential in addressing challenges and advancing technologies. Organic group incorporation was a popular method for improving the catalytic performance of microporous materials by obtaining new physicochemical properties. Thus, inorganic–organic hybrid materials compose the ultimate material.[10–12] Porous materials with adjustable tunability can be synthesized, allowing the manufacturing of materials with specified functionality. This is helpful in building materials, where both strength and weight are important factors, because it allows for their successful use in a variety of disciplines, contributing to improvements in technology, industry, and scientific study.[13–15]

The results of condensation reactions between primary amines and ketones or aldehydes are known as Schiff bases, and they are used extensively in biological activity, corrosion, medicine, analytical chemistry, photochromic, and catalysis.[16,17] Schiff–base complexes based on transition metals are increasingly sought-after coordination complexes that have played an important role in

R. Prajapati, R. Bandyopadhyay
Department of Chemistry
School of Energy Technology
Pandit Deendayal Energy University
Raisan, Gandhinagar, Gujarat 382426, India
E-mail: rajib.bandyopadhyay@sot.pdpu.ac.in

J. Chaudhari, P. Paredi, D. Vyawhare, K. Shah, M. Bandyopadhyay
Institute of Infrastructure
Technology, Research and Management
IITRAM
Maninagar, Ahmedabad, Gujarat 380026, India
E-mail: krupashah@iitram.ac.in
mahuyabandyopadhyay@iitram.ac.in

N. Tsunoji
Graduate School of Advanced Science and Engineering
Hiroshima University
Higashi-Hiroshima 739-8527, Japan

N. Tsunoji
Center for Research on Green Sustainable Chemistry
Tottori University
4-101 Koyama-cho Minami, Tottori 680-8552, Japan

R. Bandyopadhyay
Rhein-Waal University of Applied Sciences
47533 Kleve, Germany

the advancement of coordination chemistry.[18,19] The vast majority of Schiff base metal complexes are homogenous, even though these complexes have high catalytic activity efficiency and a diversity of active sites. The use of Schiff base transition-metal complexes as heterogeneous supports has centered on the development of innovative catalytic processes based on effective catalysts that are easy to recover and affordable.[20–22]

Epoxides are small compounds that possess a broad array of applications in synthetic organic chemistry react to different nucleophiles, such as alcohols, amines, water, and others.[23,24] Epoxidation has remained a popular industrial important reaction and one of the most significant transformations in organic synthesis, producing a variety of β-amino alcohols as a product.[25] Because of their medicinal, pharmacological, and biological value, β-amino alcohols are gaining popularity.[26–29] Several ways have been used, including the prominent application of β-amino alcohols in industrial applications.[30–32] Several chemicals have been found to enhance ring opening in epoxides. The ring-opening reaction of cyclohexene oxide with water in the presence of a Nafion-H-perfluorinated sulfonic acid resin catalyst yields *trans*-1,2-diol.[33,34] Traditionally, epoxide ring-opening processes are performed at increased temperatures; however, at higher temperatures, undesirable side products cannot be avoided.[35,36] Researchers have made several attempts to achieve more significant yield from epoxide ring-opening reactions in mild and solvent-free reaction systems.[30,37]

There is a substantial amount of research on the usage of Cu-complex-based heterogeneous systems in epoxide ring-opening reactions for production of significant $\beta$-amino alcohols. Dongmei Jiang et al. the usage of Cu-complex-anchored MOF in the epoxide ring-opening process.[38] M. Mar D'az-Requejo et al. developed copper-based catalysts containing polypyrazolylborate ligands for the conversion of olefins into cyclopropanes, aziridines and epoxides, and alkynes into cyclopropenes.[39] G. Olason investigated the oxidation of cyclohexene by t-butyl hydroperoxide and dioxygen, which was assisted by Cu catalyst supported by polybenzimidazole.[40] The impact of $\mu_4$-oxo-bridged copper (II) complexes in liquid-phase partial oxidation reaction of olefins was investigated by Partha Roy et al.[41] Amir Khojastehnezhad et al. used the Hummer process to synthesize graphene oxide, and the hydroxyl groups on the surface were changed to acyl chloride, and Cu(II)-tetrakis(aminophenyl)porphyrin (Cu-PPh) was immobilized to the graphene oxide's borders.[42] Clara Pereira et al. designed heterogeneous oxovanadium and copper acetylacetonate catalysts: Covalent immobilization effects in epoxidation and aziridination reactions.[43] Divya et al. created a tetranuclear Zn-complex covalently immobilized sulfopropylsilylated mesoporous silica, which was shown to be an effective material for the ring-opening reaction of epoxide with amine.[44]

Machine learning (ML) is being extensively used nowadays to understand and explore the properties of new solid catalytic materials, especially heterogeneous catalysts that lack adequate theoretical ML model. For theoretical prediction, first-principles calculated values as well as experimental values for specific catalytic reactions are required. ML with advanced computational techniques can be employed to predict quantities of interest, such as stability, activity and selectivity of heterogeneous catalysts. There are a few studies based on ML predictions of heterogeneous catalysis findings. K. Suzuki et al. analyzed catalytic reactions including methane oxidative coupling, CO oxidation, and water–gas shift, using least absolute shrinkage and selection operator regression, ridge regression, random forest (RF) regression, and extra trees regression. The work presented the difficulties and limitations of ML for heterogenous catalyst.[45] It is worth noting that Martin Hájek and collaborators recently published a *meta*-analysis of experimental data from rapeseed oil ethanolysis, which resulted in high activity and stability in the presence of a molecular sieve and evaluated the data exploring broader range of reaction conditions using linear regression (LR).[46] Minxiang Zeng et al. evaluated water cleaning reactions using several search methods, including support vector machine (SVM), k-nearest neighbors (kNN), RF, and gradient boosting (GB). They discovered that GB provided the greatest agreement on efficiency data.[47] Zhuole Lu et al. used a Gaussian process regression (GPR) model, Gaussian kernel regression, and Gaussian kernel-based SVM to recognize patterns on reaction paths. GPR performed best with a root mean square error (RMSE) of 0.30 eV, mean absolute error (MAE) of 0.09 eV, and $R^2$ greater than 0.9 for both aggregation and adsorption energy testing sets ranking.[48] **Table 1** provides a comprehensive summary of the existing literature on the application of ML in heterogeneous catalysis, highlighting key studies, experimental variables, and findings. It covers various ML approaches utilized to enhance catalyst design and predict catalytic performance. A comprehensive review cited in Table 1 highlights several key research findings which faced challenges in data quality, model interpretability, scalability, and experimental validation. Despite the advancements in ML applications for heterogeneous catalysts, there remains a gap in understanding the predictive limitations and generalizability of these models across a wider variety of catalytic systems and reaction conditions. From this point of view, we have examined the development of an effective ML predictive protocol for the ring-opening process of propylene oxide with piperidine as well as how ML models can be used to understand the qualities of a catalyst for a specific reaction. The effect of the catalytic performance using Cu-complex-incorporated base-functionalized SAPO structure was examined. In comparison to pure SAPO, the catalytic activity was observed to be improved following functionalization of the base group and the incorporation of complex. The successful incorporation of Cu complex in microporous molecular sieves was identified employing several physicochemical characterization methods. Under optimized conditions, at 90 °C for 6 h, complex-incorporated functionalized SAPO- 5 and SAPO- 34 displayed 90% and 86% conversion of propylene oxide, respectively, and 97% product selectivity. Predictive ML algorithms were used to analyze the conversion and product selectivity in heterogeneous catalysis with their variables, exploring the dependency between each variable through co-variable analysis by doing visualization inspections. The study focuses on employing the accurate predictive ML algorithms to find quality of catalyst for specific reactions by measuring their minimum error for the reliability of ML models. The pure,

**Table 1.** Previous work on applications of machine learning methods on different heterogenous catalysts.

| Catalyst | Reaction | Model | Experimental variables | Output | Practicability of ML | Results | Reference |
|---|---|---|---|---|---|---|---|
| CaO catalyst | Transesterification | Response surface methodology(RSM) | Methanol to oil ration, catalyst concentration (wt%), reaction time | Yield | RSM methods use quadratic regression models to analyze variable correlations and identify key quality characteristics in biodiesel production. | The model shows M:O Ratio and reaction time strongly affect the process, with CaO yielding 93% to 75% over five cycles. | [60] |
| Zirconocene catalysts | α-Olefin polymerization | Artificial neural network (ANN) | Reaction space | Reaction rate constant | ANN predicted polymer properties from kinetic constants, offering insight reactor design and polymer development. | $R^2$—0.9987 | [52] |
| Hydroxyapatite (HAp)/chitosan composite | Adsorption | Adaptive neuro-fuzzy inference systems (ANFIS) | pH, shaker velocity, temperature, amount of adsorbent, initial concentration | Adsorption capacity | Neuro-fuzzy modeling effectively predicted lead adsorption by the nanocomposite, while the nano-hydroxyapatite/ chitosan composite exhibited superior lead ion removal capacity. | Total average error: −0.0646%, absolute error: −4.2428%. | [53] |
| Germanium-containing Zeolite | – | Random forest (RF), decision tree (DT), natural language processing (NLP) | Synthesis parameters | Zeolite's topology | A data extraction using NLP and analysis of zeolite synthesis data to predict zeolite topology from synthesis conditions, paving the way for rational zeolite design and synthesis. | DT R score–0.97 | [61] |
| Polyaniline | – | Gradient boost (GB), tree, SVM, and ensemble-based regressor models | S impedance and phase value | pH values | The smart sensing platform developed for urine pH with over 98% accuracy using gradient boost and is accessible to users via a local web app, enabling effective urinary pH detection. | RMSE (GB): 0.07622 | [62] |
| Zeolites | – | Not mentioned | pH control, heating/ cooling | Synthesis link | Machine learning (ML) enables predictive modeling and optimization of zeolite synthesis. | ML offers the "missing link" to rationalize zeolite synthesis. | [63] |
| X and Y faujasite zeolite | Adsorption | Multilinear regression (MLR), ANFIS | Temperature, pressure, and molecular weight of cations | Adsorption capacity | ANFIS accurately predict the adsorption of methane gas on X and Y zeolites in the presence of the substituted cations. | $R^2$–0.9997, RMS–0.0321, MAE–0.0238, mean absolute relative error%–1.8517 | [64] |
| Ziegler–Natta (ZN) | Production of polyolefins | Genetic algorithm (GA) | Not mentioned | Adsorption states | GA and density-functional calculation developed the methodology for nonempirical structure determination. | ZN catalyst particles and models complex supported catalysts. | [65] |

amine-functionalized, and Cu-complex-immobilized SAPO- 5 and SAPO- 34 have been abbreviated as S-5, S-34, S-5-N, S-34-N, S-5-N-Cu, and S-34-N-Cu, respectively. Catalyst reaction predictions are complex because they often involve nonlinear relationships between reaction variables such as temperature, pressure, reactants, catalyst composition, etc., and reaction outcomes such as conversion and selectivity. Extending LR by adding polynomial features could capture nonlinear relationships. Hence, this model can be considered as the basic model and can be used before testing more complex algorithms. The basic trends in catalyst reaction can be well understood with simple analysis if this model performs well. However, exhibiting less accuracy, more sophisticated algorithms like SVM and kNN would be required to apply. SVM can perform well with high-dimensional data and can find optimal boundaries when the relationship between input variables and catalytic outcomes is not straightforward. It is possible to avoid overfitting with this algorithm and therefore it can be suitable for the cases dealing with a limited dataset as shown in this work. kNN is also capable of capturing complex, nonlinear patterns in the catalytic dataset and can provide predictions based on the closest data points in the training set. This is beneficial for catalytic processes, where local clusters in data may impact conversion and selectivity. Due to these features of SVM and kNN along with their ability to perform regression for limited datasets having nonlinear relationship, they are considered and used extensively in this work.

## 2. Results and Discussion

A variety of analytical methods were used to comprehensively characterize the synthesized hybrid materials. Powder X-ray diffraction (XRD) was used to confirm the base functionality and the presence of foreign entities, as shown in **Figure 1**. It was discovered that after the base functionalization or metal complex, there is a loss of peak intensity due to decrease in the scattering contrast between pore and pore wall after each modification. In case of SAPO -5-N-Cu, two additional peaks at around 9° and 11° 2$\theta$, and for SAPO-34-N-Cu at around 11° 2$\theta$, were observed respectively which match with pure Cu complex, indicating the successful anchoring of Cu-complex onto the surface of the porous material.

The morphology of modified SAPOs was studied using field-emission scanning electron microscopy (FE-SEM) as shown in **Figure 2**A,B. The cubic morphology of base-functionalized SAPO-34 shows that the form and size of the SAPO-34 did not change considerably after modification. The morphology of S-5-N-Cu is nearly similar to that of pure SAPO-5. After the inclusion of the Cu complex, partial aggregation is seen in the S-5-N-Cu catalyst.

**Figure 3** and **Table 2** describe nitrogen sorption analysis of SAPO-34 and SAPO-5. Brunauer-Emmett-Teller (BET) surface areas were found to be 447 and 354 $m^2 g^{-1}$, for S-34 and S-5, respectively, with pore volumes of 0.12 and 0.13 $cm^3 g^{-1}$. Surface area and other textural parameters were significantly reduced after metal complex inclusion. This is consistent with published data and examines the high quality of the SAPO-34 and SAPO-5 samples. All surface attributes were reduced after metal complex immobilization, indicating effective integration of guest functionality onto the silica basis. The inductively coupled plasma-optical emission spectrometry (ICP-OES) technique was used to determine the metal content, which is summarized in Table 2. The Si/Cu ratio in SAPO is 36.50 for base-functionalized SAPO materials, and 30. 20 for base-functionalized SAPO- 5 materials, demonstrating the immobilization of the mononuclear Cu complex on base-modified microporous silica. Both the materials show a type I isotherm with a representative hysteresis loop. The existence of nano-porosity is confirmed by the presence of hysteresis loop in all the materials. The BJH technique was used to get the pore size distribution curve (**Figure 4**) of Cu-incorporated materials. Thermogravimetric analysis (TGA) was also done to determine the thermal behavior of the modified materials, (**Figure 5**). The Cu-complex revealed four stages with a 72% weight decrease from 198 to 494 °C. However, after immobilization in microporous silica, the thermal constancy of the modified materials was considerably improved, with ≈20% weight reduction in the 25–780 °C range.

### 2.1. Catalytic Activity Test

After evaluating catalytic activities in the epoxide ring-opening reaction of propylene oxide with piperidine utilizing, Cu-complex-incorporated SAPO catalysts, and also without catalysts, the effectiveness of the catalysts using post-synthetic approach is clearly visible. In the process of ring-opening reaction of propylene oxide for 6 h, the required amount of pure SAPO materials was employed, and it is confirmed from **Figure 6** that untreated SAPO material exhibited the least conversion when compared to metal-complex-incorporated materials. A total of 55% of the reactants were transformed by the S-34-N material, whereas 42% were converted by the S-5-N material. Only 12% conversion was attained in absence of a catalyst. A considerable increase in catalytic activity was observed using Cu-metal-complex-immobilized SAPOs, 90% and 86% conversion with S-34-N-Cu and S-5-N-Cu catalysts, individually.

#### *2.1.1. Mechanism*

**Scheme 1** provides a schematic representation of the proposed mechanistic route for the ring opening of propylene oxide employing microporous SAPO-34 and SAPO-5 materials integrated with Cu complex.[49] The sixth vacant site of the Cu complex, coordinates with propylene oxide via an acid–base interaction to boost the electrophilic character of the carbon, resulting in the hexa-coordinated transition state. The resulting carbocation is then attacked by piperidine or another nucleophile to yield the result. Proton transfer takes place from nitrogen to oxygen producing a product, leaving the catalyst free.

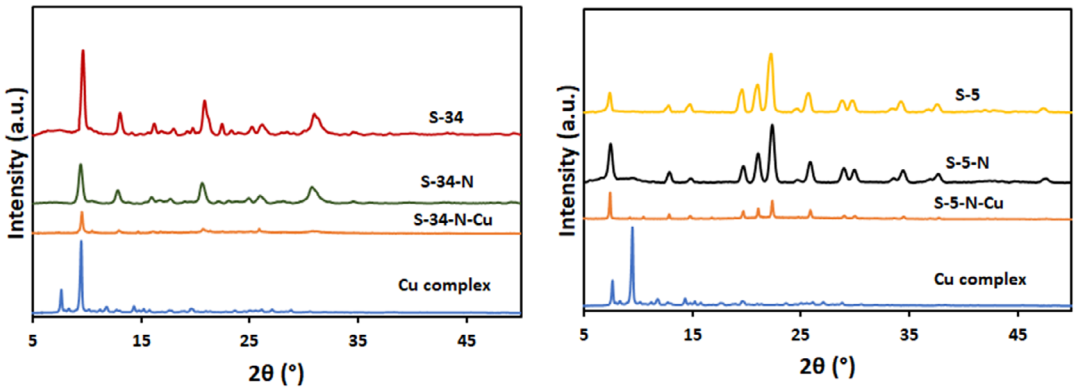


**Figure 1.** XRD pattern of a pure, base-functionalized, Cu-complex-incorporated microporous SAPO-34 and SAPO-5 materials.

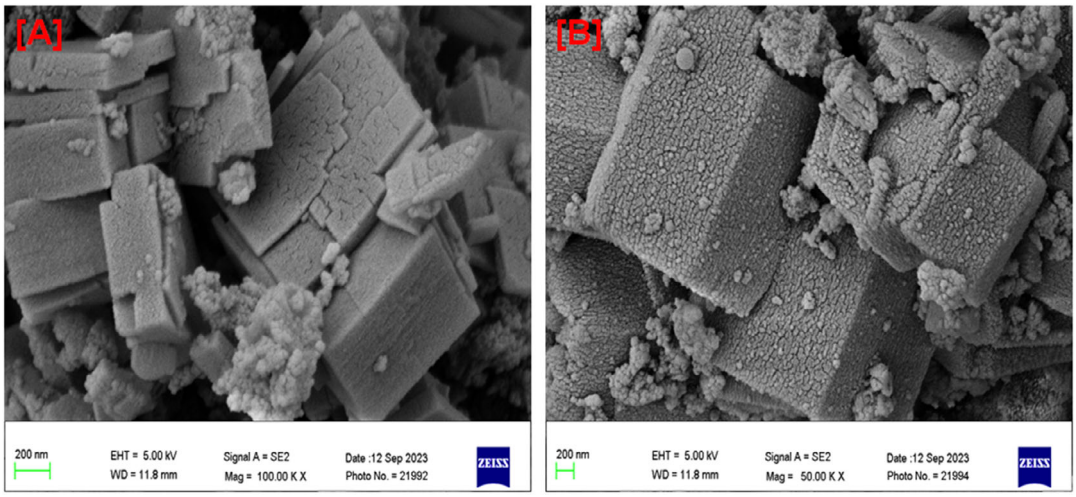


**Figure 2.** SEM images of A) S-34-N-Cu and B) S-5-N-Cu.

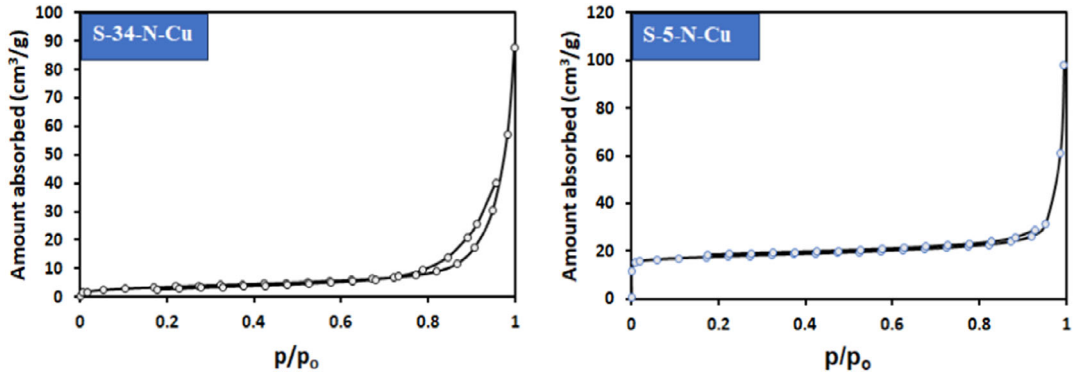


**Figure 3.** BET isotherm of Cu-complex-incorporated base-functionalized SAPO-34 and SAPO-5.

**Table 2.** Textural properties of calcined and modified SAPO-5 and SAPO-34 materials.

| Catalyst | BET surface area [$m^2 g^{-1}$] | Pore volume [$cm^3 g^{-1}$][a)] | Si/Cu ratio[b)] |
|---|---|---|---|
| S-34 | 447 | 0.12 | – |
| S-5 | 354 | 0.13 | – |
| S-34-N-Cu | 13 | 0.11 | 36.50 |
| S-5-N-Cu | 67 | 0.102 | 30.20 |

[a)]Determined by BJH method; [b)]determined by ICP-OES.

## 2.2. Optimization of Reaction Conditions

Optimization of reaction conditions focuses on adjusting key factors like catalyst quantity, reaction time, and temperature. Fine-tuning of these parameters enhances reaction efficiency, leading to improved performance and better control over product outcomes.

### *2.2.1. Catalyst Amount*

The catalyst amount was varied from 20 to 40 mg to optimize the catalytic system at a temperature of 90 °C for 6 h reaction period with piperidine to achieve the highest conversion. As the quantity of catalyst increases, the reactant's conversion also improves as illustrated in **Figure 7**. From 20 to 40 mg of catalyst, piperidine conversion improved from 68% to 90% for S-34-N-Cu and 60% to 86% for S-5-N-Cu.

### *2.2.2. Reaction Temperature*

The conversion of piperidine at various reaction temperatures is shown in **Figure 8**. Using 40 mg of catalyst, the reaction temperature was adjusted from 80 to 90 °C for piperidine, in 6 h reaction time. For S-34-N-Cu, it was found that as the temperature increased, the conversion rate improved as well; for example, at 80 °C, the conversion rate was 84%, and at higher temperatures, it climbed to 90%. For S-5-N-Cu, the conversion rate improved from 78% to 86% by increasing the temperature.

### *2.2.3. Reaction Time*

To further optimize the process, the reaction was carried out at various reaction periods. The results are shown in **Figure 9**. S-5-N-Cu showed 86% and S-34-N-Cu reached 90% conversion after 6 h of reaction under 90 °C temperature, using 40 mg catalyst,

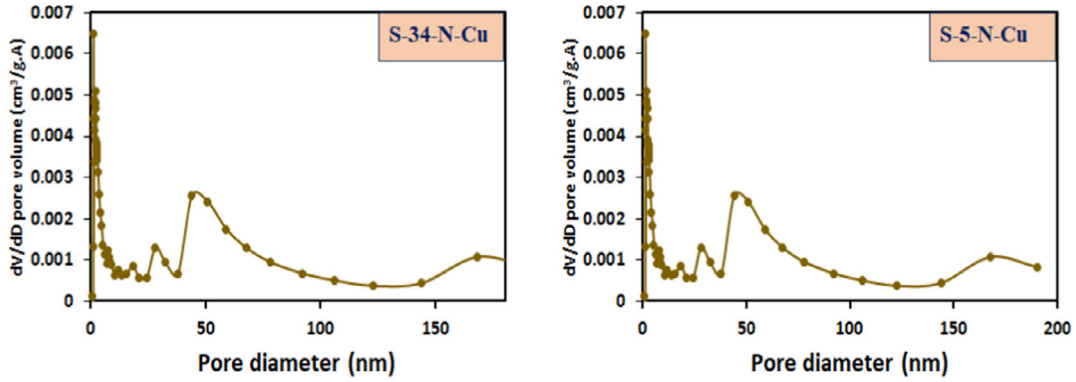


**Figure 4.** Pore size distribution of S-34-N-Cu and S-5-N-Cu.

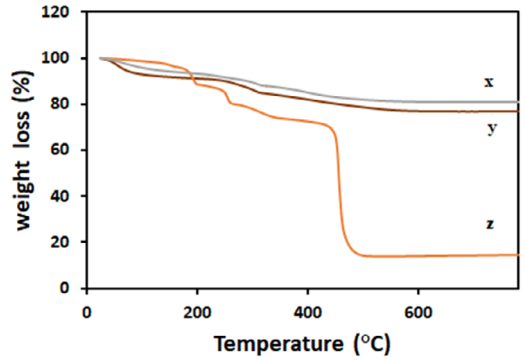


**Figure 5.** TGA of (x) S-34-N-Cu, (y) S-5-N-Cu, and (z) Cu complex.

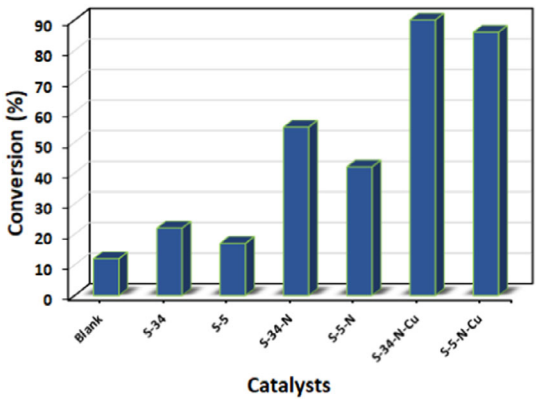


**Figure 6.** Piperidine conversion using blank, S-34, S-5, S-34-N, S-5-N, S-34-N-Cu, S-5-N-Cu. Reaction conditions: 40 mg catalyst, 90 °C temperature, and 6 h reaction time.

and 88% and 90% conversion, respectively, after 12 h reaction time with S-5-N-Cu and S-34-N-Cu. From the previously performed different parameters, the optimized condition for epoxide ring-opening reaction using hybrid SAPOs was found to be 40 mg catalyst amount, 90 °C reaction temperature, and 6 h reaction time.

#### *2.2.4. Recyclability Test*

The XRD patterns for the recycled S-34-N-Cu and S-5-N-Cu catalysts are presented in **Figure 10**. After each reaction cycle, the solid catalyst was recovered through centrifugation, washed with methanol, and dried. The XRD analysis of the spent catalysts revealed no change in peak intensity and no peak shifting, indicating that the structural integrity of the catalysts remained intact after reaction. These findings confirm that S-34-N-Cu and S-5-N-Cu are both active and stable catalysts for the epoxide ring-opening reaction, demonstrating their potential for reuse in catalytic applications.

The acidity of the modified SAPO materials was evaluated, as shown in **Table 3**. The total acidity values for S-34-N-Cu and S-5-N-Cu were found to be 0.13 and 0. 11 mmol $g^{-1}$, respectively. The turnover frequency (TOF) values were calculated to determine the efficiency of the active sites in both catalysts. A high TOF value was observed, indicating excellent catalytic activity. Notably, the TOF values for both catalysts were found to be identical and uniform, suggesting that the accessibility of active sites in both materials are similar. This observation is further supported by the catalytic activity results, which confirm that both catalysts exhibit comparable performance. The S-34-N-Cu and S-5-N-Cu catalysts, which had undergone extensive characterization, were investigated for 6 h in a liquid-phase medium at ambient temperature for the synthesis of 1-(piperidine-1-yl) propan-2-ol and 2-(piperidine-1-yl)propan-1-ol. The findings established under various experimental conditions are replicated in **Table 4**. The input data contains various variables as amount of catalyst, temperature, time, conversion, selectivity. Few of these values are shown later for reference.

### 2.3. Data Preparation and ML Models

#### *2.3.1. Data Preparation*

The chemical process feeds the information to the ML models with attributes as catalyst name, amount (mg), temperature (°C), time (min), reactant 1, reactant 2, and corresponding selectivity conversion. The dataset was prepared based on the experiment conducted in the lab. The chemical process of catalyst design to its characterization to retrieve their conversion and selectivity is time consuming process, which is crucial to gather more information based on the catalyst materials. Experiments were conducted to gather more information from

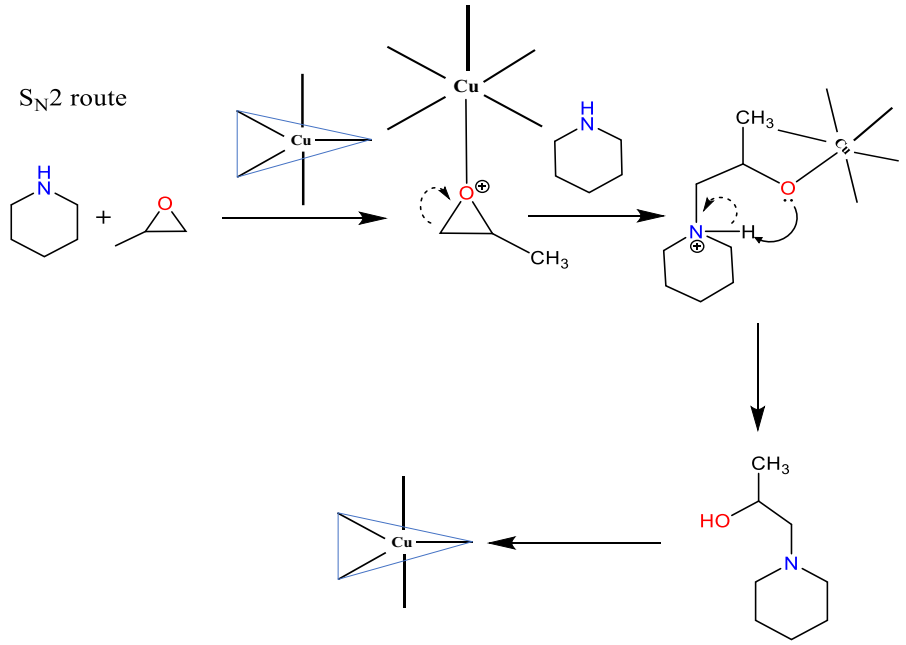


**Scheme 1.** Proposed reaction mechanism of epoxide ring opening of propylene oxide with piperidine.

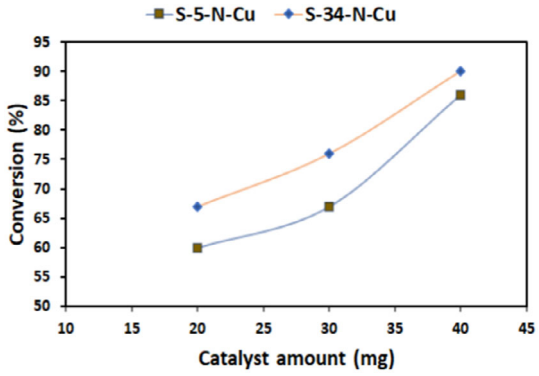


**Figure 7.** Piperidine conversion using different catalyst amount of S-34-N-Cu and S-5-N-Cu. Reaction conditions: 90 °C temperature and 6 h reaction time.

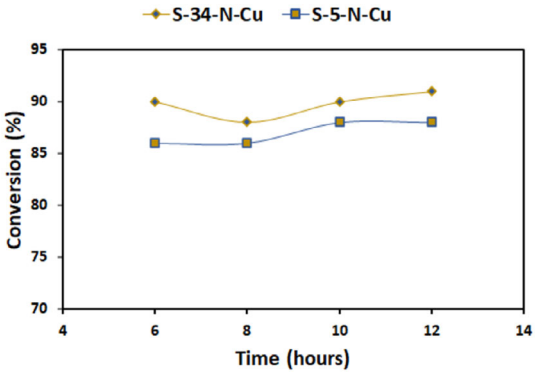


**Figure 9.** Piperidine conversion using reaction time of S-34-N-Cu and S-5-N-Cu. Reaction conditions: 40 mg catalyst amount and 90 °C temperature.

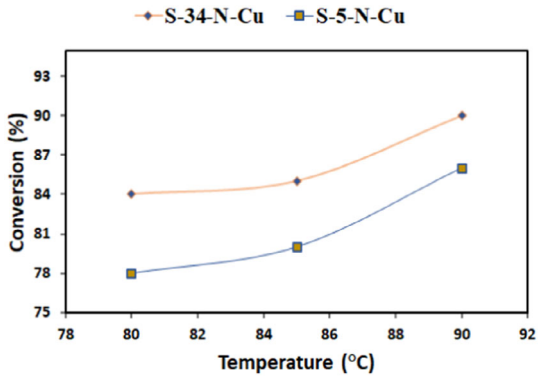


**Figure 8.** Piperidine conversion using reaction temperature of S-34-N-Cu and S-5-N-Cu. Reaction conditions: 40 mg catalyst amount and 6 h reaction time.

which total 499 samples were utilized to feed into ML models. The use of ML models with the prepared experiment data is used to train the model for a similar process on a large scale (industrial application) to be used in the future. A well-trained model with the experimental data can be utilized in the future for predicting conversion and selectivity from the given material information.

Initially, two datasets were created pertaining to the catalyst S-34-N-Cu with 249 samples and S-5-N-Cu with 250 samples. Data augmentation approach was utilized with these two datasets by applying Gaussian noise to enlarge the data samples. The total of 498 and 500 samples were generated for each dataset respectively. Thus, the total samples considered for the training were 998. In the earlier stage of data augmentation, the analysis was carried out for variable correlation and feature selection. To find out correlation between the variables, variable correlation analysis was

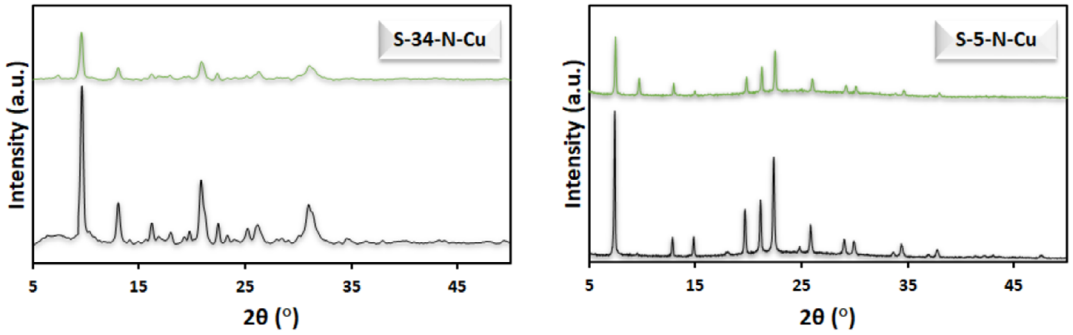


**Figure 10.** XRD of recycled S-34-N-Cu and S-5-N-Cu.

**Table 3.** Conversion, acidity, and TOF with different catalyst amounts.

| Catalyst | Catalyst amount [g] | Conversion [%] | Acidity [mmol $g^{-1}$] | TOF [$h^{-1}$] |
|---|---|---|---|---|
| S-34-N-Cu | 0.02 | 67 | 0.13 | 423 |
| | 0.03 | 76 | | 320 |
| | 0.04 | 90 | | 284 |
| | 0.05 | 87 | | 220 |
| S-5-N-Cu | 0.02 | 60 | 0.11 | 419 |
| | 0.03 | 67 | | 313 |
| | 0.04 | 86 | | 300 |
| | 0.05 | 84 | | 235 |

**Table 4.** Epoxide ring-opening reaction on pure and modified SAPO-34 catalysts.

| Catalyst | Amount [mg] | Temp. [°C] | Time [min] | Conversion [%] | Selectivity [%] |
|---|---|---|---|---|---|
| SAPO-34 | 40 | 90 | 360 | 20 | 96 |
| SAPO-34-N | 40 | 90 | 360 | 52 | 95 |
| SAPO-34-N-Cu | 5 | 90 | 360 | 11 | 95 |
| SAPO-34-N-Cu | 10 | 90 | 360 | 23 | 96 |
| SAPO-34-N-Cu | 15 | 90 | 360 | 35 | 96 |

carried out by plotting correlation matrix for each variable as shown in **Figure 11**. Moreover, in feature selection, the two variables were dropped such as reactant 1 and reactant 2 as their value were constant throughout the experiment and they are not correlated with each other. With these changes, the finalized features were found as amount (mg), temperature (°C), and time (min) as shown in **Figure 12**. Similarly, pair plot was designed between the selected features as shown in **Figure 13**. At the end of data augmentation process, normalization of the data was carried out. During the feature selection, conversion and selectivity were taken separately as y variables of the models to train the model precisely. To feed normalized data, a standard scaling approach was utilized as shown in **Table 5**. After feature selection, augmentation, and normalization, the input data shape of catalyst S-34-N-Cu was found as (498,3) and that of S-5-N-Cu was found as (500,3). Further, the datasets were divided into train and test data in the ratio of 80:20, where 80% data were utilized for training along with cross validation and 20% data were utilized for testing.

### *2.3.2. ML Models*

In this research work, ML algorithms were applied to train and test the augmented datasets to predict the values of conversion and selectivity of S-34-N-Cu and S-5-N-Cu, respectively. The ML algorithms such as LR, SVM, and then kNN were utilized. Primarily, these algorithms were trained separately for conversion and selectivity. To obtain accurate results, tenfold cross validations were utilized during the training process. During each fold, mean-squared error (MSE), mean absolute percentage error (MAPE), and R-score (R-squared) error was obtained between predicted values from the model versus observed values acquired from the experiment. The MAPE was shown with line graphs in Figure 20–22 for both the catalysts. At the end, these same errors were observed with the test data for all the algorithms, and the obtained results were noted in **Table 6**.

### *2.3.3. LR*

Conversion and selectivity are dependent variables, for which LR builds a linear model to predict these values based on independent variables such as amount (mg), temperature (°C), and time (min). A model was trained separately for S-34-N-Cu and S-5-N-Cu, for their conversion and selectivity. Initially, LR model was least accurate; however, to maximize the accuracy and minimize the error, polynomials features were supplied to the LR model. This would further ensure the better fitment of the model, since the relationship between the reaction variables and reaction outcomes is nonlinear. The transformation of normalized data to polynomial normalized data reduces the error at certain point where accurate results can be obtained. Further, these data were supplied to the model, where tenfold cross validation was utilized to train the LR model. At every fold MSE, MAPE, and R score were calculated. After the last fold, average value was calculated for each error. After the training, predictions were made on test data with the trained model. Moreover, MSE, MAPE, and R score between the actual and the predicted values obtained from the experiments and the trained model respectively were observed. This process was repeated with other catalyst S-5-N-Cu to predict its conversion and selectivity. The corresponding results for each catalyst are mentioned in Table 6. To provide visual inspection, regression

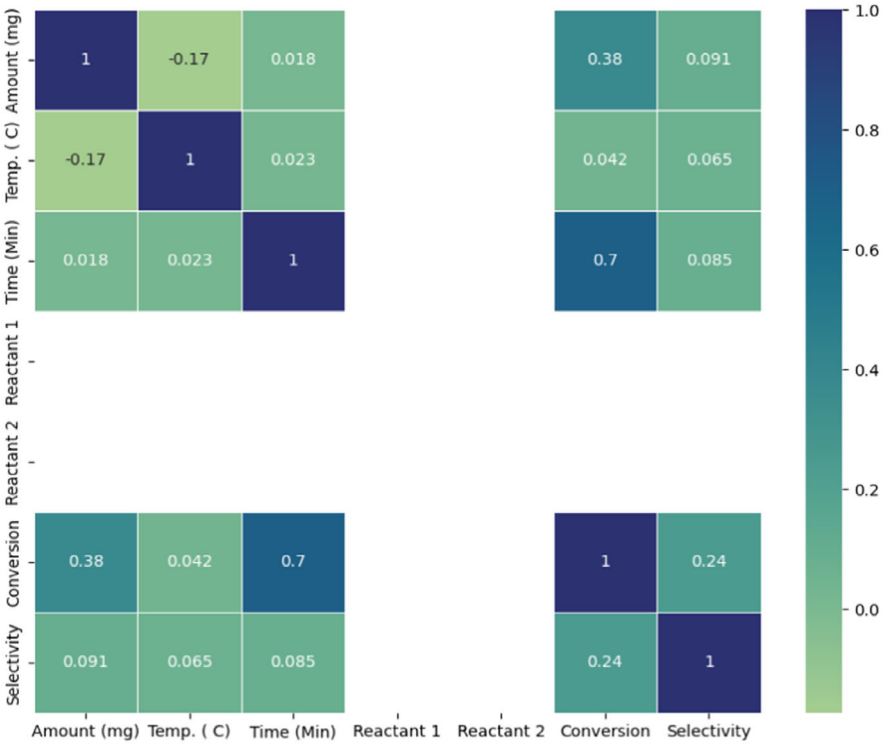


**Figure 11.** Correlation matrix of all variables.

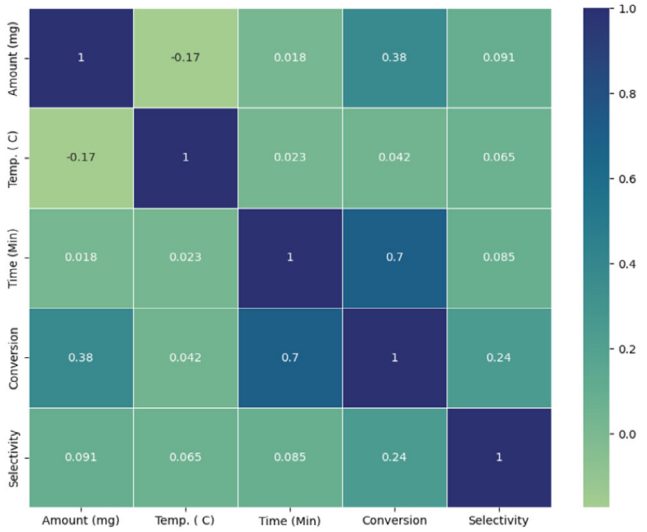


**Figure 12.** Correlation matrix of selected variables.

graphs are plotted between actual versus predicted values for both the variables separately as shown in **Figure14** and **15** pertaining to S-34-N-Cu and S-5-N-Cu, respectively.

### *2.3.4. SVM*

Since this ML study aims at providing accurate regressor model of conversion and selectivity for the given catalysts, SVM regressor was utilized with normalized data. Similar process of LR was followed while training the model with normalized features and tenfold cross validation. SVM focuses on minimizing the distance between predicted values obtained through the model and actual values acquired through experiment within the margin for accurate results. The best results were observed by considering parameters as C value and kernel selection. The best parameters were identified using grid search and these values are, C = 100 and kernel = radial basis function. Based on these parameters, accurate results were generated. During the training with tenfold cross validations, errors such as MSE, MAPE, and R score were calculated. Similar error observations were noted with the test data after completing the training process and the same is mentioned in Table 6. Similarly, this process was repeated with other catalyst S-5-N-Cu to predict its conversion and selectivity. The corresponding results for each catalyst are mentioned in Table 6. To provide visual inspection, regression graphs are plotted between actual versus predicted values for both the variables separately as shown in **Figure 16** and **17** pertaining to S-34-N-Cu and S-5-N-Cu, respectively.

### *2.3.5. kNN*

The kNN approach is more suitable for classification, however, it also supports the regression tasks. Since building regressor model is the main aim of this study, kNN model was utilized as a regressor. The result of the kNN model was observed with the test data, which outperforms for S-34-N-Cu. To acquired minimum errors, kNN model was trained with tenfold cross validations, and the results were observed with test data MSE, MAPE, and R score. The parameters that play an important role

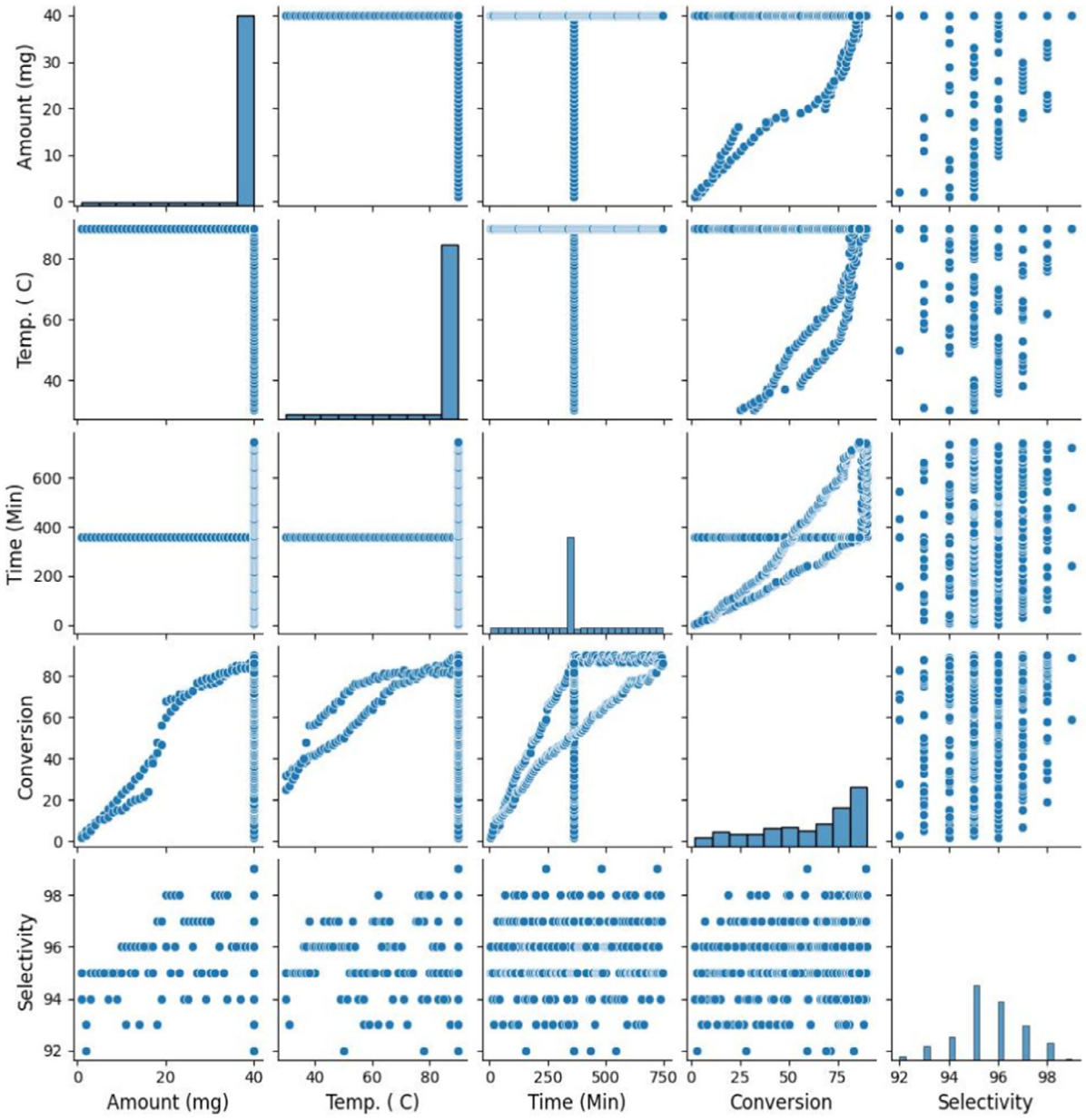


**Figure 13.** Pair plot to describe the relationship between variables.

**Table 5.** Scaled data of catalyst.

| Amount [mg] | Temperature [°C] | Time [min] | Conversion [%] | Selectivity [%] |
|---|---|---|---|---|
| 0.1988 | 0.3499 | −0.0294 | 20 | 96 |
| 0.1988 | 0.3499 | −0.0294 | 52 | 95 |
| −4.573 | 0.3499 | −0.0294 | 11 | 95 |
| −3.892 | 0.3499 | −0.0294 | 23 | 96 |
| −3.21 | 0.3499 | −0.0294 | 35 | 96 |

while training the model, that were kth value, distance matrix, and weights. The model was trained with different values using grid search and the final parameter values were $k = 5$, distance = Manhattan, and weights = distance; on which the model outperforms. Similarly, this process was repeated with other catalyst S-5-N-Cu to predict its conversion and selectivity. The corresponding results for each catalyst are mentioned in Table 6. To provide visual inspection, regression graphs are plotted between actual versus predicted values for both the variables separately as shown in **Figure 18** and **19** pertaining to S-34-N-Cu and S-5-N-Cu, respectively.

Toward the end, performance of the model is evaluated based on MSE, MAPE, and R score of the test data as mentioned in Table 6. For S-34-N-Cu, minimum difference was observed in kNN for conversion and selectivity. For S-5-N-Cu, the SVM performed well. Moreover, MSE, MAPE, and R score were also obtained for the trained datasets. From the results, it can be inferred that overall SVM was performed well for both the

**Table 6.** Observation table for MSE, MAPE, R score.

| | | LR | | SVM | | KNN | |
|---|---|---|---|---|---|---|---|
| | | Conversion | Selectivity | Conversion | Selectivity | Conversion | Selectivity |
| S-34-N-Cu | MSE | 18.314 | 1.502 | 1.57 | 0.905 | 0.946 | 0.387 |
| | MAPE | 0.133 | 0.010 | 0.043 | 0.007 | 0.010 | 0.004 |
| | R score | 0.971 | 0.098 | 0.997 | 0.456 | 0.998 | 0.767 |
| S-5-N-Cu | MSE | 52.695 | 1.168 | 12.764 | 1.062 | 13.481 | 0.383 |
| | MAPE | 0.243 | 0.008 | 0.071 | 0.007 | 0.025 | 0.004 |
| | R score | 0.915 | 0.036 | 0.979 | 0.05 | 0.978 | 0.659 |

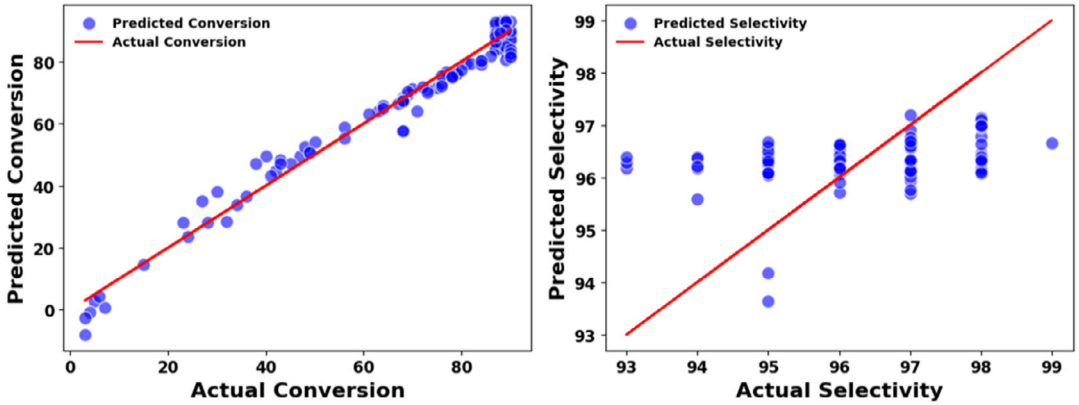


**Figure 14.** Regression plot of actual and predicted value for conversion and selectivity of S-34-N-Cu using linear regression.

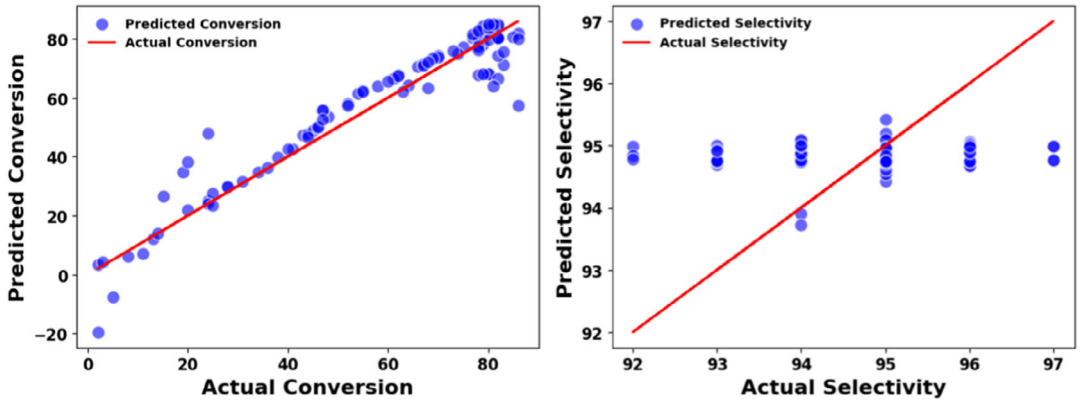


**Figure 15.** Regression plot of actual and predicted value for conversion and selectivity of S-5-N-Cu using linear regression.

catalysts. The visual inspection of only MAPE is shown (from **Figure 20** to **22**) for brevity.

## 3. Methodology

The methodology comprises three sections: the synthesis and characterization study of the materials is the first part, where second part involves observing catalytic reaction through optimization of various reaction conditions and the third part, consisting of application of various ML methods. The flowchart of the proposed methodology is shown in **Figure 23**.

### 3.1. Synthesis of Catalyst and Characterization

#### *3.1.1. Synthesis of SAPOs*

The procedures mentioned in our previous study[50] were used to synthesize the catalyst materials. Aluminum iso-propoxide and *o*-phosphoric acid were used as aluminum and phosphorus

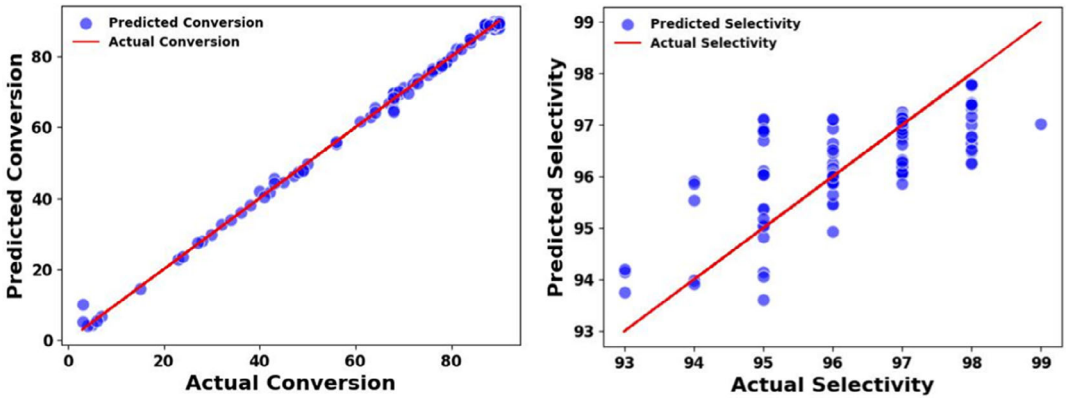


**Figure 16.** Regression plot of actual and predicted value for conversion and selectivity of S-34-N-Cu using SVM.

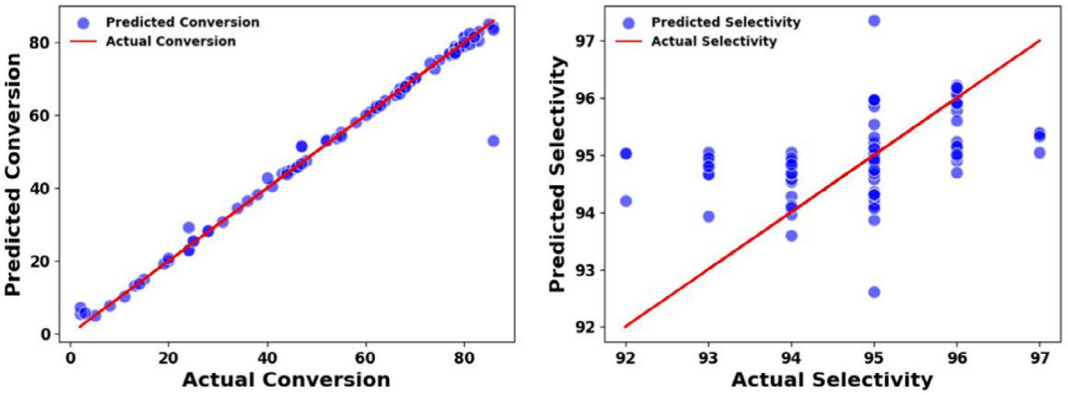


**Figure 17.** Regression plot of actual and predicted value for conversion and selectivity of S-5-N-Cu using SVM.

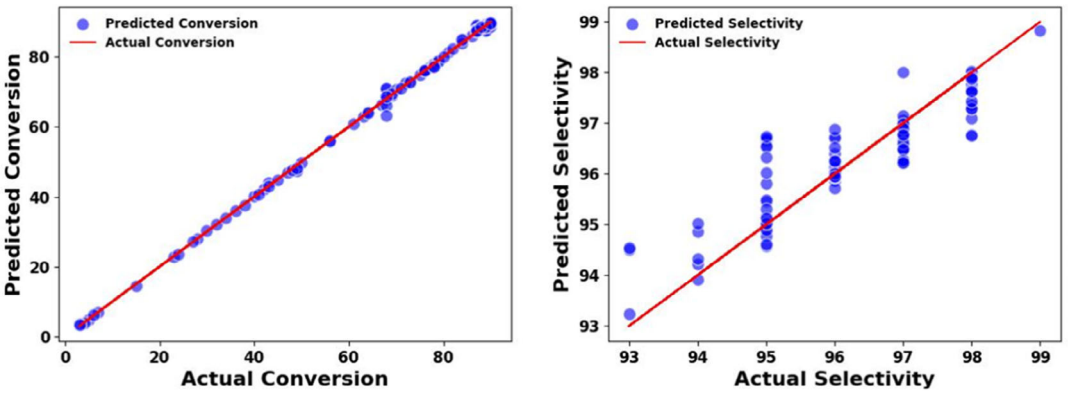


**Figure 18.** Regression plot of actual and predicted value for conversion and selectivity of S-34-N-Cu using kNN.

sources, respectively. In a typical synthesis, aluminum iso-propoxide was mixed with half of the Milli-Q water at room temperature with continuous stirring. The remaining water and *o*-phosphoric acid were then added dropwise, followed by colloidal silica and template. The gel mixture was transferred to a Teflon-lined autoclave and crystallized at 48 °C for 24 h. The product was filtered, washed, dried, and calcined at 823 K to remove the template.

### *3.1.2. Amine Functionalization*

The amine functionalization of SAPOs was done as per the earlier reported procedure.[51] The catalyst support was dried at 70 °C for 4 h. The material was then mixed with (3-Aminopropyl)triethoxy silane in toluene and refluxed at 120 °C for 12 h. The resulting functionalized SAPO-5 and SAPO-34 materials were filtered, rinsed with toluene, and air-dried.

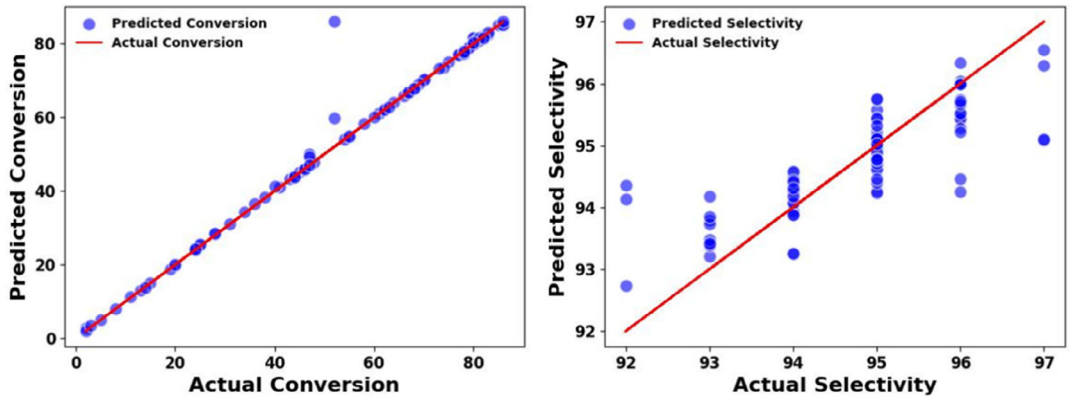


**Figure 19.** Regression plot of actual and predicted value for conversion and selectivity of S-5-N-Cu using kNN.

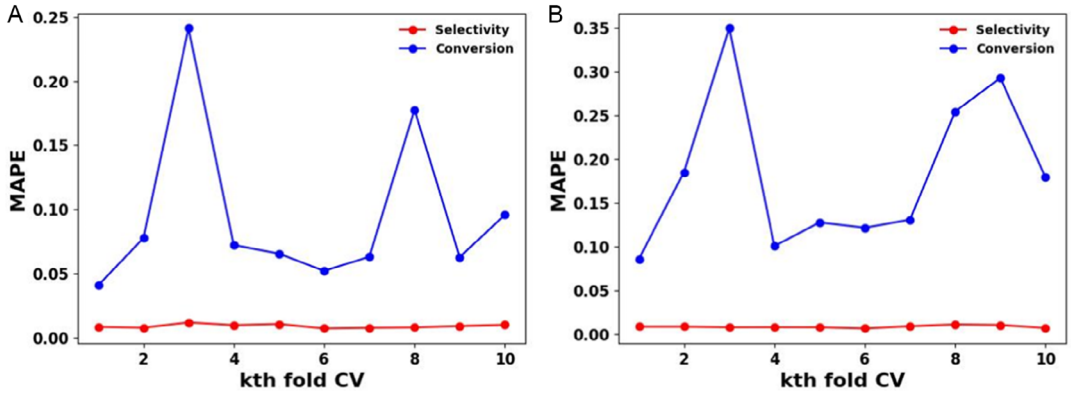


**Figure 20.** Tenfold cross-validation line graph of linear regression for A) S-34-N-Cu and B) S-5-N-Cu.

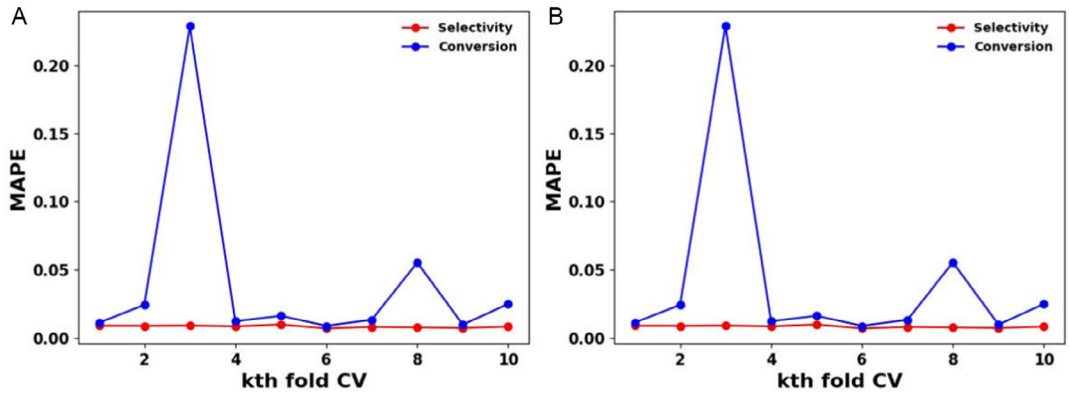


**Figure 21.** Tenfold cross-validation line graph of support vector machine for A) S-34-N-Cu and B) S-5-N-Cu.

### *3.1.3. Preparation and Incorporation of Copper Complex into Material*

The procedure involved dissolving the ligand 2,9-dimethyl-1,10-phenanthroline in methanol and adding copper (II) nitrate salt to the mixture, stirring the mixture for an appropriate time and filtering, washing with methanol, and placing the liquid for crystallization to produce green precipitate that was filtered and formed into diamond-shaped crystals which were suitable for single-crystal X-ray diffraction.[52] The microporous SAPO-34 and SAPO-5 were prepared using a process described in the literature.[52] The supporting materials were prepared using a well-known literature procedure. The approach for immobilizing the Cu-complex was followed as per the literature[53] procedure. The functionalized material and Cu-complex were combined in a specific proportion in toluene solvent for 16 h reaction time preceding filtering, washing, and drying.

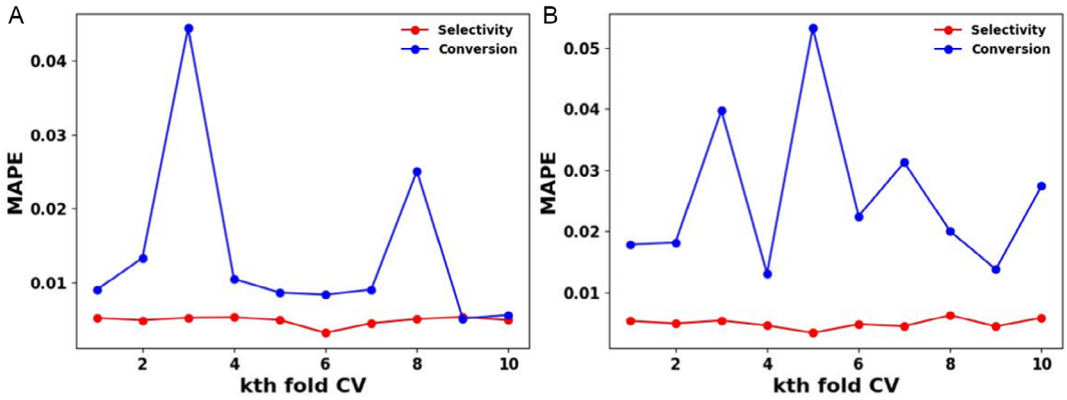


**Figure 22.** Tenfold cross-validation line graph of k-nearest neighbor for A) S-34-N-Cu and B) S-5-N-Cu.

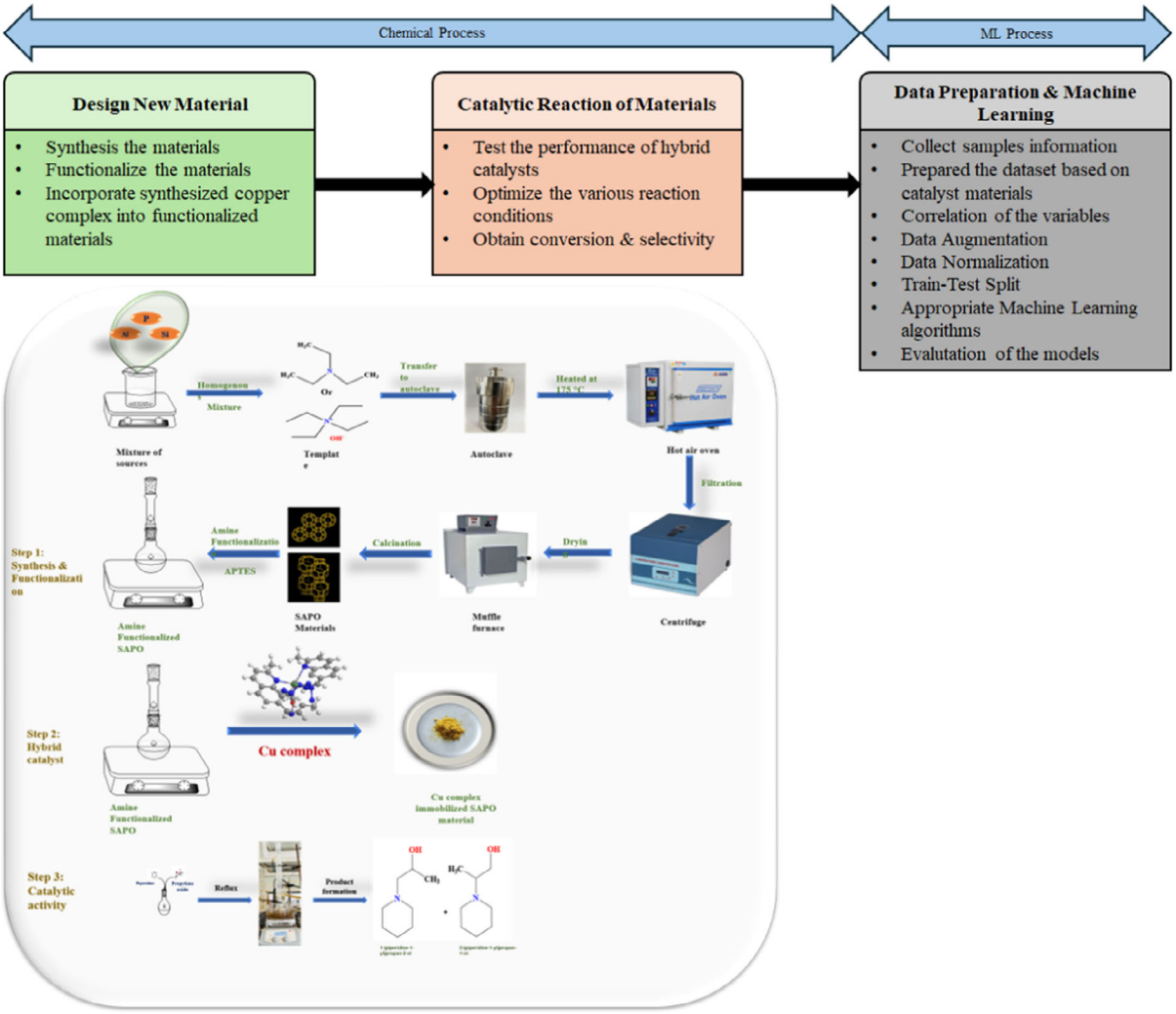


**Figure 23.** Schematic view of data flowchart for proposed methodology.

### 3.2. Characterization

XRD patterns were obtained using a powder X-ray diffractometer (Bruker, PHASER) with graphite-monochromatized Cu Kα radiation at 30 kV and a tube current of 10 mA. The crystal morphology of the sample was observed using SEM (Hitachi S-4800). TGA was carried out using a Hitachi instrument. A dry air flow of 30 mL $min^{-1}$ was used to heat the sample from room temperature to 800 °C at a rate of 10 °C $min^{-1}$. Nitrogen (−196°C) adsorption–desorption isotherm study was performed on samples that

had been pretreated at 150 °C for 4 h using a Micromeritics-3 flex 3500 apparatus.

### 3.3. Catalytic Reaction

A Cu-complex-encapsulated hybrid SAPO material was used to perform a solvent-free ring-opening reaction of propylene oxide with piperidine. The hybrid material was activated for an hour at 80 °C before the reaction, and the needed amount of catalyst was combined with propylene oxide and piperidine at different temperatures and reaction periods. The catalyst was removed from the reaction mixture, and the product was analyzed using a gas chromatograph (Thermo Fisher Trace-1310, TG 5 column). Piperidine was used as a nucleophile to open the ring of propylene oxide over a hybrid catalyst (**Scheme 2**). To improve the efficiency of the epoxide ring-opening reaction in the presence of a Cu-complex-immobilized base-functionalized SAPO catalyst, several factors such as the amount of catalyst, temperature, and reaction time on the performance of the heterogeneous catalyst were studied. The following are the optimized reaction conditions: 40 mg catalyst, 6 h reaction duration, and 90 °C temperature.

### 3.4. Data Preparation and ML Models

The proposed study employs various ML algorithms to build regressor models for predicting the performance of the catalysts for various reaction conditions, and for evaluating results obtained from such regressor models with that obtained through optimization of reaction conditions. Further this section divides in two parts: Section 5.4.1 explains about data preparation and Section 5.4.2 explains ML algorithms and their evaluation. Initially, preparation of the dataset is to be done to feed into ML algorithms for predicting the performance of catalyst such as conversion and selectivity with various reaction parameters. The dataset was prepared based on the conducted chemical experiment having reaction parameters (termed as variables) such as catalyst type, amount (mg), temperature (°C), time (min), reactant 1, reactant 2, and reaction outcomes such as conversion and selectivity. The regressor models aim to make predications on catalyst reactions, that are complex because they often involve nonlinear relationships between reaction variables and reaction outcomes. To address this, initially variable correlation analysis is carried out, followed by visual inspections with correlation matrix and pair plot, that can help to eliminate the non-useful variables.

### 3.5. Data Preparation

#### *3.5.1. Variable Correlation*

The correlation matrix provides a brief overview of the relationships between variables in the dataset. By visualizing the correlation coefficients between each pair of variables, it is possible to understand the key structure and dependencies within the data. High positive correlations indicate variables that tend to move together, while negative correlations suggest variables that move in opposite directions. The correlation matrix pertaining to catalyst dataset utters about the factors that may influence the reaction outcomes, conversion and selectivity. In addition, the pair plot provides a visual representation of the relationships between multiple pairs of variables in the dataset. By visualizing scatter plots, it is possible to understand the dataset distributions, patterns, outliers, and clusters within the data.

#### *3.5.2. Data Augmentation*

Data augmentation approach aims to enlarge the data particularly when the size of data is limited. Given the relatively small size of the experimental dataset, comprising 499 rows, its capacity to effectively train ML model is limited. To address this challenge, a data augmentation technique was implemented. Moreover, applying this approach during the training process can prevent overfitting and can enhance the model ability to perform effectively on the unseen data. To enlarge the experimental data, which is numerical in nature, noise can be added by utilizing Gaussian noise that follows the normal distribution of data based on their mean ($\mu$) and standard deviation ($\sigma$), respectively.

#### *3.5.3. Data Normalization*

To ensure consistent and optimal performance, feature scaling was conducted. Standard scaling was employed to normalize the features within the dataset, preventing certain features from dominating others during model training. This also ensures convergence toward an optimal solution. Mathematically, random noise injection involves adding random values within a specified

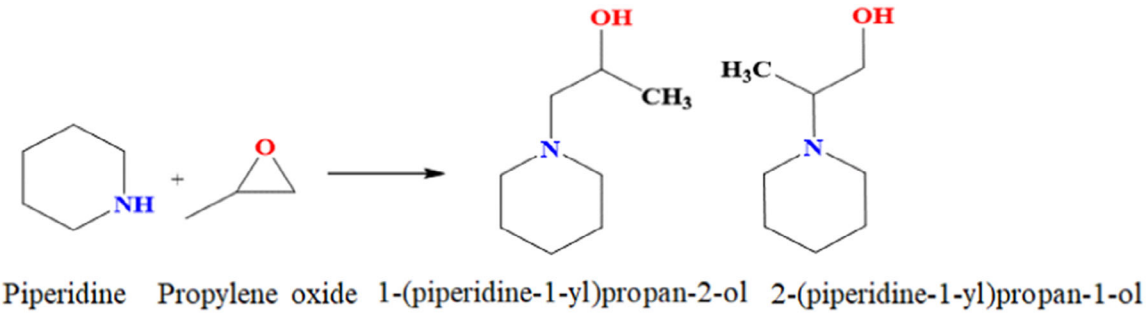


**Scheme 2.** Ring-opening reaction of propylene oxide with piperidine.

range to the dataset, while standard scaling transforms the dataset such that each feature $x_i$ is scaled according to the formula $x_i = \frac{(x_i - \mu)}{\sigma}$ where $\mu°$ represents the mean and $\sigma°$ denotes the standard deviation of the feature. Further to address complex nonlinear relationship, polynomial features can be utilized. This approach transforms the original features into the polynomial combinations, that allows to capture nonlinearity within the given data and to improve the potential of the model performance. For further evaluation, the dataset was divided into training and testing sets, with 20% of the dataset allocated for testing purposes and 80% for training.

### 3.6. ML Models

Appropriate selection of algorithms is necessary based on dataset. As discussed in Section 1, for performing regression, to forecast conversion and selectivity, suitable algorithms are identified as LR, SVM, and kNNs. To ensure accurate model performance, a tenfold cross-validation approach is employed during training phase. This validation approach divides the datasets into 10 equally sized folds, that utilized 9 folds for training and remaining for validation; and iterates 10 times by supplying each fold for validation. The average performance across all folds provides the reliable estimation of the model performance ability.

### 3.7. LR

LR is a fundamental method in predictive modeling and is employed alongside SVM in this study due to its simplicity and interpretability.[54,55] Since, LR provides indication of the strength and direction of the relationships between variables, it can be considered as a valuable algorithm for predictive modeling tasks. For the said work, LR establishes a relationship between the reaction variables and the reaction outcomes by fitting a linear equation as shown later to predict the data points.

$$y = \beta_0 + \beta_1 x_1 + \beta_2 x_2 + \ldots_{..} + \beta_n x_n + \varepsilon \tag{1}$$

where $y$ is the predicted reaction outcomes, $x_i$ is the reaction variables, $\beta_i$ is the regression coefficients, and $\varepsilon°$ represents the error term. The coefficients $\beta_i$ are estimated using the method of least squares, minimizing the sum of squared differences between the observed and predicted values. To minimize the error and to increase the dependency between the variables considered, polynomial features can be supplied.

### 3.8. SVM

SVM algorithm is employed in the proposed study due to its versatility in handling regression tasks effectively.[56,57] Unlike its traditional classification application, SVM in the regression task aims to predict continuous outcomes by fitting a hyperplane that captures the underlying patterns in the data. By implementing various kernel functions, such as linear, polynomial, or Gaussian kernels; complex nonlinear relationships between reaction variables and reaction outcomes can be captured by SVM. The regularization parameter C plays a crucial role in minimizing the prediction error and maximizing the margin between data points. SVM attempts to minimize the difference between the predicted and actual values of the reaction outcomes by appropriate training. Therefore, valuable insights for catalyst predictions can be achieved. The SVM model can be trained using the regression formulation

$$\min_{W,b,\xi} \frac{1}{2}||W||^2 + C\sum_{i=1}^{n}\xi_i, \text{subject to} y_i - W^T\phi(x_i) - b \le \varepsilon + \xi_i, \xi_i \ge 0 \tag{2}$$

where $W$ is the weight vector, $b$ is the bias term, $\xi_i$ is slack variables, $\phi(x_i)$ is the feature mapping function, and $\varepsilon$ is the epsilon-insensitive loss parameter.

### 3.9. kNN

The kNNs algorithm is a simple and powerful nonparametric method used for both classification and regression tasks where it stands out for its simplicity and effectiveness in prediction tasks.[58,59] kNN operates by identifying the kNNs of a given data point in the feature space, typically determined by Euclidean or Manhattan distance. For each data point $x$ in the feature space, its Euclidean or Manhattan distance to every other data point $x_i$ in the dataset is calculated by given formula, respectively.

$$d(x, x_i) = \sqrt{\sum_{j=1}^{n}(x_j - x_{ij})^2} \tag{3}$$

$$d(x, x_i) = \sum_{j=1}^{n}|x_j - x_{ij}| \tag{4}$$

This nonparametric approach is particularly advantageous when the underlying data distribution is complex or unknown.

#### *3.9.1. Evaluation of the Models*

The aforementioned three algorithms are compared for their effectiveness in predicting conversion and selectivity. The performance of each model was evaluated using three metrics: MSE, MAPE, and R-score value. MSE measures the average squared difference between the predicted and actual values of reaction outcomes. A lower MSE signifies closer alignment between predicted and observed values. MAPE metric evaluates the accuracy of predicting models by measuring the average percentage difference between predicted and actual values. R-score (R-squared) calculation is the proportion of variance in the dependent variable that is explained by the independent variables. A higher R-squared value signifies a stronger correlation between predicted reaction outcomes obtained through ML model and observed values of chemical reaction.

## 4. Conclusion

The proposed research is based on synthesis and catalytic application of a mixed ligand copper (||) complex and grafting of the complex in amine-functionalized SAPO-5 and SAPO-34 followed by data visualization and preprocessing of ML-based approaches to predict conversion and selectivity of heterogeneous catalysts. The hybrid material was used as catalyst in epoxide ring-opening reaction of propylene oxide. The designed hybrid catalyst has been found to be extremely active and truly heterogeneous in nature showing 90% conversion of propylene oxide with very high selectivity of product. Copper complex significantly enhances catalytic activity by amplifying the electrophilic properties of carbon, enabling a more efficient ring opening of epoxides and accelerating the reaction rate. The preprocessed data is then fed to various ML algorithms such as LR, SVM, and kNN to predict the quality of catalysts for specific reactions. The performance of the considered algorithms was evaluated through visual inspection and utilizing quantitative metrics such as MSE, MAPE, and R score. Redundant variables were identified and eliminated through a correlation matrix and pair plot analysis to improve the quality of the dataset. All models were trained precisely using tenfold cross validation on experimental data acquired from the synthesis process. Initially, LR struggled to capture the nonlinear relationship between the reaction variables and outcomes due to its linear nature. However, SVM and kNN performed well for the given objective for predicting the quality of catalyst for specific reactions and effectively captured nonlinearity with the limited data. The visual inspection of line graphs identified low errors during training of both the models whereas, regression graph identified a close match between predicted and actual values that demonstrated better efficiency of the models in predicting catalyst conversion and selectivity during test. The novelty of the work lies in the prepared copper (II) complex and its immobilization in microporous support for excellent catalytic activity in epoxide ring-opening reaction at ambient temperature and examined ML that brings advanced computational techniques to predict conversion and selectivity of heterogeneous catalysts.

## Acknowledgements

M.B. acknowledges the SERB-DST SURE Project "SUR/2022/000353" for its financial assistance. R.P. expresses deep gratitude to the SRDC-PDPU, Gandhinagar, for the support in FE-SEM measurements and Dr. S.D. of IITRAM for his assistance in the lab.

## Conflict of Interest

The authors declare no conflict of interest.

## Author Contributions

**Rohit Prajapati**: formal analysis (lead); investigation (lead); methodology (lead); and writing—original draft (lead). **Jetal Chaudhari**: data curation (equal); methodology (supporting); and software (lead). **Parikshit Paredi**: investigation (supporting) and methodology (supporting). **Daksh Vyawhare**: methodology (supporting). **Nao Tsunoji**: data curation (supporting); investigation (supporting); and resources (supporting). **Rayan Bandyopadhyay**: software and editing. **Krupa Shah**: conceptualization (equal); data curation (equal); methodology (equal); and writing—review and editing (equal). **Rajib Bandyopadhyay**: conceptualization (equal); methodology (equal); and writing—review and editing: (equal). **Mahuya Bandyopadhyay**: conceptualization (lead); project administration (lead); supervision (lead); visualization (lead); and writing—review and editing (lead).

## Data Availability Statement

The data that support the findings of this study are available from the corresponding author upon reasonable request.

**Keywords:** data augmentation · hybrid porous materials · k-nearest neighbors · linear regression · ring-opening reactions of epoxide

[1] C. Becker, *Encycl. Interfacial Chem.* **2018**, 99.
[2] F. Zaera, *Catal. Lett.* **2012**, *142*, 501.
[3] M. Pandey, N. Tsunoji, R. Bandyopadhyay, S. Das, M. Bandyopadhyay, *Hybrid Adv.* **2023**, *2*, 100030.
[4] Y. Li, Z. Y. Fu, B. L. Su, *Adv. Funct. Mater.* **2012**, *22*, 4634.
[5] F. Thielmann, *J. Chromatogr. A.* **2004**, *1037*, 115.
[6] F. Sun, J. Gao, X. Liu, Y. Yang, S. Wu, *J. Chem. Eng.* **2012**, *290*, 116.
[7] Sastre, G., Lewis, D. W., Catlow, C. R. A., *J. Phys. Chem. B.* **1997**, *101*, 5249.
[8] R. B. Borade, A. Clearfield, *J. Mol. Catal.* **1994**, *88*, 249.
[9] S. U. H. Bakhtiar, S. Ali, Y. Dong, X. Wang, F. Yuan, Z. Li, Y. Zhu, *J. Porous Mater.* **2018**, *25*, 1455.
[10] B. Hatton, K. Landskron, W. Whitnall, D. Perovic, G. A. Ozin, *Acc. Chem. Res.* **2005**, *38*, 305.
[11] U. Schubert, N. Hüsing, A. Lorenz, *Chem. Mater.* **1995**, *7*, 2010.
[12] D. Zhou, X. B. Luo, H. L. Zhang, C. Dong, Q. H. Xia, Z. M. Liu, F. Deng, *Microporous Mesoporous Mater.* **2009**, *121*, 194.
[13] G. Zhang, P. Zhao, L. Hao, Y. Xu, *J. CO2 Util.* **2018**, *24*, 22.
[14] K. M. Parida, S. Mallick, G. C. Pradhan, *J. Mol. Catal. A Chem.* **2009**, *297*, 93.
[15] S. T. Yang, J. Y. Kim, J. Kim, W. S. Ahn, *Fuel* **2012**, *97*, 435.
[16] Y. Wu, W. Wang, L. Liu, S. Zhu, X. Wang, E. Hu, K. Hu, *ChemistryOpen* **2019**, *8*, 333.
[17] A. Z. El-Sonbati, W. H. Mahmoud, *Appl. Organomet. Chem.* **2019**, *33*, e5048.
[18] L. H. Abdel-Rahman, R. M. El-Khatib, L. A. Nassr, A. M. Abu-Dief, F. E. D. Lashin, *Acta A Mol. Biomol. Spectrosc.* **2013**, *111*, 266.
[19] S. Yamada, *Coord. Chem. Rev.* **1999**, *190*, 537.
[20] Y. Yang, Y. Zhang, S. Hao, J. Guan, H. Ding, F. Shang, Q. Kan, *Appl. Catal. A Gen.* **2010**, *381*, 274.
[21] J. Rakhtshah, S. Salehzadeh, M. A. Zolfigol, S. Baghery, *J. Coord. Chem.* **2017**, *70*, 340.
[22] K. C. Gupta, A. K. Sutar, *Coord. Chem. Rev.* **2008**, *252*, 1420.
[23] Y. Liu, R. C. Klet, J. T. Hupp, O. Farha, *ChemComm.* **2016**, *52*, 7806.
[24] E. N. Jacobsen, *Acc. Chem. Res.* **2000**, *33*, 421.
[25] C. Wang, L. Luo, H. Yamamoto, *Acc. Chem. Res.* **2016**, *49*, 193.
[26] J. Rehdorf, M. D. Mihovilovic, U. T. Bornscheuer, *Angew. Chem. Int. Ed.* **2010**, *26*, 4506.
[27] G. H. Posner, D. Z. Rogers, *J. Am. Chem.* **1977**, *99*, 8208.
[28] D. Bhuyan, L. Saikia, D. K. Dutta, *Appl. Catal. A.* **2014**, *487*, 195.
[29] I. Matos, P. D. Neves, J. E. Castanheiro, E. Perez-Mayoral, *Appl. Catal. A* **2012**, *439*, 24.
[30] G. Sekar, V. K. Singh, *J. Org. Chem.* **1999**, *64*, 287.
[31] S. Roy, B. Banerjee, N. Salam, A. Bhaumik, S. M. Islam, *ChemCatChem* **2015**, *7*, 2689.
[32] M. M. Islam, P. Bhanja, M. Halder, S. K. Kundu, A. Bhaumik, S. M. Islam, *RSC Adv.* **2016**, *6*, 109315.

[33] V. Mirkhani, S. Tangestaninejad, B. Yadollahi, L. Alipanah, *Tetrahedron* **2003**, *59*, 8213.
[34] J. G. Smith, *Synthesis* **1984**, *1984*, 629.
[35] D. J. Darensbourg, M. W. Holtcamp, *Coord. Chem. Rev.* **1996**, *153*, 155.
[36] H. Y. Ji, B. Wang, L. Pan, Y. S. Li, *Green Chem.* **2018**, *20*, 641.
[37] A. Kamal, B. R. Prasad, A. M. Reddy, M. N. Khan, *Catal. Commun.* **2007**, *8*, 1876.
[38] D. Jiang, A. Urakawa, M. Yulikov, T. Mallat, G. Jeschke, A. Baiker, *Chem. Eur. J.* **2009**, *15*, 12255.
[39] M. M. Díaz-Requejo, P. J. Pérez, *J. Org. Chem.* **2001**, *617*, 110.
[40] G. Olason, D. C. Sherrington, *React. Funct. Polym.* **1999**, *42*, 163.
[41] P. Roy, M. Nandi, M. Manassero, M. Riccó, M. Mazzani, A. Bhaumik, P. Banerjee, *Dalton Trans.* **2009**, *43*, 9543.
[42] A. Khojastehnezhad, M. Bakavoli, A. Javid, M. M. Khakzad Siuki, F. Moeinpour, *Catal. Lett.* **2019**, *149*, 713.
[43] C. Pereira, K. Biernacki, S. L. Rebelo, A. L. Magalhaes, A. P. Carvalho, J. Pires, C. Freire, *J. Mol. Catal. A Chem.* **2009**, *312*, 53.
[44] D. Jadav, P. Shukla, R. Bandyopadhyay, Y. Kubota, S. Das, M. Bandyopadhyay, *Mol. Catal.* **2020**, *497*, 111220.
[45] K. Suzuki, T. Toyao, Z. Maeno, S. Takakusagi, K. I. Shimizu, I. Takigawa, *ChemCatChem* **2019**, *11*, 4537.
[46] M. Hájek, F. Skopal, L. Čapek, M. Černoch, P. Kutálek, *Energy* **2012**, *48*, 392.
[47] Z. Lu, S. Yadav, C. V. Singh, *Catal. Sci. Technol.* **2020**, *10*, 86.
[48] M. Zeng, S. Yuan, D. Huang, Z. Cheng, *ACS Appl. Mater. Interfaces.* **2019**, *11*, 40099.
[49] R. Prajapati, N. Tsunoji, M. Bandyopadhyay, R. Bandyopadhyay, *J. Porous Mater.* **2023**, *30*, 2087.
[50] P. Paredi, M. Pandey, N. Tsunoji, R. Prajapati, S. Das, M. Bandyopadhyay, *Mol. Catal.* **2023**, *547*, 113357.
[51] A. Dhakshinamoorthy, M. Alvaro, H. Garcia, *Chem. Eur. J.* **2010**, *16*, 8530.
[52] B. A. Rizkin, R. L. Hartman, *Chem. Eng. Sci.* **2019**, *210*, 115224.
[53] Z. Jensen, E. Kim, S. Kwon, T. Z. Gani, Y. Román-Leshkov, M. Moliner, E. Olivetti, *ACS Cent. Sci.* **2019**, *5*, 892.
[54] S. Zhang, X. Li, M. Zong, X. Zhu, D. Cheng, *ACM Trans. Intell. Syst. Technol.* **2017**, *8*, 1.
[55] G. Guo, H. Wang, D. Bell, Y. Bi, K. Greer, *On the Move to Meaningful Internet Systems 2003: CoopIS, DOA, and ODBASE* (Eds: R. Meersman, Z. Tari, D. C. Schmidt), Springer, Berlin Heidelberg **2023**, pp. 986–996.
[56] S. Yue, P. Li, P. Hao, *Appl. Math. Ser. B* **2003**, *18*, 332.
[57] K. S. Durgesh, B. Lekha, *J. Theor. Appl. Inf. Technol.* **2010**, *12*, 1.
[58] J. Groß, *Springer Sci. Bus. Med.* **2003**, 175.
[59] X. Su, X. Yan, C. L. Tsai, *Wiley Interdiscip. Rev. Comput. Stat.* **2012**, *4*, 275.
[60] N. S. El-Gendy, S. S. Abu Amr, H. A. Aziz, *Energy Sources, Part A: Recovery, Utili., Environ. Effects* **2014**, *36*, 1615.
[61] A. Sadeghizadeh, F. Ebrahimi, M. Heydari, M. Tahmasebikohyani, F. Ebrahimi, A. Sadeghizadeh, *J. Environ. Manage.* **2019**, *232*, 342.
[62] H. Rezaei, M. Rahmati, H. Modarress, *Neural Comput. Appl.* **2017**, *28*, 301.
[63] M. Moliner, Y. Román-Leshkov, A. Corma, *Acc. Chem. Res.* **2019**, *52*, 2971.
[64] G. Takasao, T. Wada, A. Thakur, P. Chammingkwan, M. Terano, T. Taniike, *Acs Catalysis* **2019**, *9*, 2599.
[65] R. Prajapati, M. Pandey, N. Tsunoji, R. Bandyopadhyay, M. Bandyopadhyay, *Mol. Catal.* **2023**, *550*, 113599.

Manuscript received: November 20, 2024
Revised manuscript received: March 26, 2025
Version of record online: